Analyzing rain erosion using a Pulsating Jet Erosion Tester (PJET)
Effect of droplet impact frequencies and dry intervals on incubation times

Verma, Amrit Shankar; Wu, Chun Yen; Díaz, Miguel Alonso; Teuwen, Julie J.E.

DOI
10.1016/j.wear.2024.205614

Publication date
2025

Document Version
Final published version

Published in
Wear

Citation (APA)
Verma, A. S., Wu, C. Y., Díaz, M. A., & Teuwen, J. J. E. (2025). Analyzing rain erosion using a Pulsating Jet Erosion Tester (PJET): Effect of droplet impact frequencies and dry intervals on incubation times. *Wear*, *562-563*, Article 205614. https://doi.org/10.1016/j.wear.2024.205614

Wear 562–563 (2025) 205614

Contents lists available at ScienceDirect

Wear

journal homepage: www.elsevier.com/locate/wear

Analyzing rain erosion using a Pulsating Jet Erosion Tester (PJET): Effect of droplet impact frequencies and dry intervals on incubation times

Amrit Shankar Verma [a,b,*], Chun-Yen Wu [b], Miguel Alonso Díaz [b], Julie J.E. Teuwen [b]

[a] Department of Mechanical Engineering, The University of Maine, Orono, ME 04473, USA
[b] Faculty of Aerospace Engineering, Delft University of Technology (TU Delft), The Netherlands

ARTICLE INFO

Keywords:
Leading edge erosion
PJET
Coating
Impact loads
Wind turbines
Operation and maintenance

ABSTRACT

Accelerated laboratory testing is essential to understand the rain erosion behavior of coated samples applied to the leading edge surface of a wind turbine blade. This study investigates the impact of droplet impact frequencies and dry intervals on the incubation time for damage on polyurethane-coated samples using a Pulsating Jet Erosion Tester (PJET). A novel theoretical model for water slug volume is introduced, allowing for a more accurate comparison across different impact velocities and frequencies. The effect of dry intervals on coating performance is quantified, revealing that longer dry intervals and shorter pre-dry rain exposure can significantly increase the number of impacts a coating can withstand before damage. The study challenges the traditional continuous impingement testing by demonstrating that dry intervals can extend incubation time by a factor of three to five. Additionally, this paper proposes a recalibrated approach to PJET testing, which better mimics the cyclic nature of real-world rainfall, leading to improved predictive models for material degradation. The findings emphasize the importance of considering the visco-elastic behavior of coatings and the role of intermittent rain exposure in erosion testing, offering invaluable insights for designing future PJET test parameters.

1. Introduction

The demand for sustainable power generation sources has led to the growth of wind turbines and the wind energy market. The installation of onshore and offshore wind turbines has increased by about 10%–11% every year for the last few years [1], and it accounted for about 15% of the energy generated in Europe in 2023 [2]. Current trends involve large-size rotor blades, with blade lengths reaching 100–123 m [3,4] and maximum tip speed ranging in the order of 75 to 110 m/s [5]. These high tip speeds of the blades cause high velocity impacts with hydrometeors such as rain droplets and hail during operations and can result in leading edge erosion (LEE) of wind turbine blades, see Fig. 1. Repetitive high-velocity rain droplet impacts cause degradation at the leading edge of the wind turbine blade (LEE) through roughening and damaging the blade surface, eventually resulting in material removal. This can turn into a significant reduction in the aerodynamic performance of the turbines and decrease of the overall annual energy production [6]. Furthermore, LEE has repercussions on the maintenance and repair costs of the blades, which is a significant portion of the total operation and maintenance cost of wind farms [7,8]. To protect wind turbine blades made of composite materials from damage caused by leading edge erosion (LEE), a protective coating is usually applied. The most advanced solution in the industry for erosion protection is the use of polyurethane (PU)-based leading edge protection (LEP) systems [9]. These protection systems are multilayered and are composed of putty, pore filler, primer, and coating and are applied to enhance adhesion to the blade substrate [10]. In addition to polyurethane (PU)-based coatings, other coatings like thermoplastic shields are also available.

Wind turbine manufacturers face the challenge of accurately assessing and comparing the erosion behavior of different coating systems. To do this, they use erosion testing facilities that perform accelerated testing. Various experimental setups are employed to study the blade coating systems' durability and resistance against rain erosion. The most commonly used ones are the pulsating water jet erosion tester (PJET) [13–18] and the whirling arm rain erosion tester (WARER), [14,19–21] see Fig. 2. Although both these test set-ups are based on accelerated testing, there are differences in terms of how the samples are tested. The WARER is a testing device consisting of one or more rotating arms on which a coated sample is placed. The arm rotates the sample under controlled rainy conditions, mimicking real-life rainfall

* Corresponding author at: Department of Mechanical Engineering, The University of Maine, Orono, ME 04473, USA.
E-mail addresses: amrit.verma@maine.edu (A.S. Verma), chunyenwu.me06@nctu.edu.tw (C.-Y. Wu), M.AlonsoDiaz@student.tudelft.nl (M.A. Díaz), j.j.e.teuwen@tudelft.nl (J.J.E. Teuwen).

https://doi.org/10.1016/j.wear.2024.205614
Received 14 April 2024; Received in revised form 20 October 2024; Accepted 26 October 2024
Available online 7 November 2024

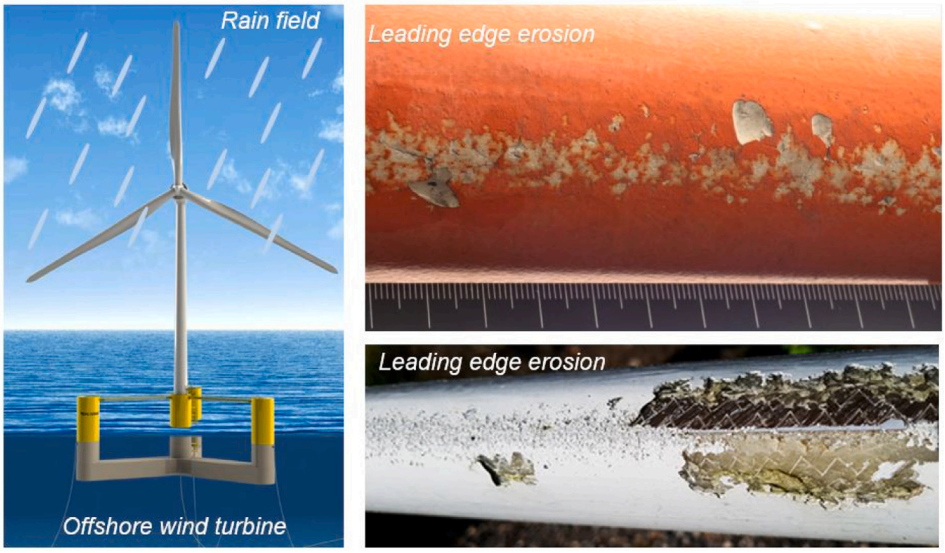

Fig. 1. Example of leading edge erosion on WTBs.
Source: TNO, DURALEDGE Project [11,12].

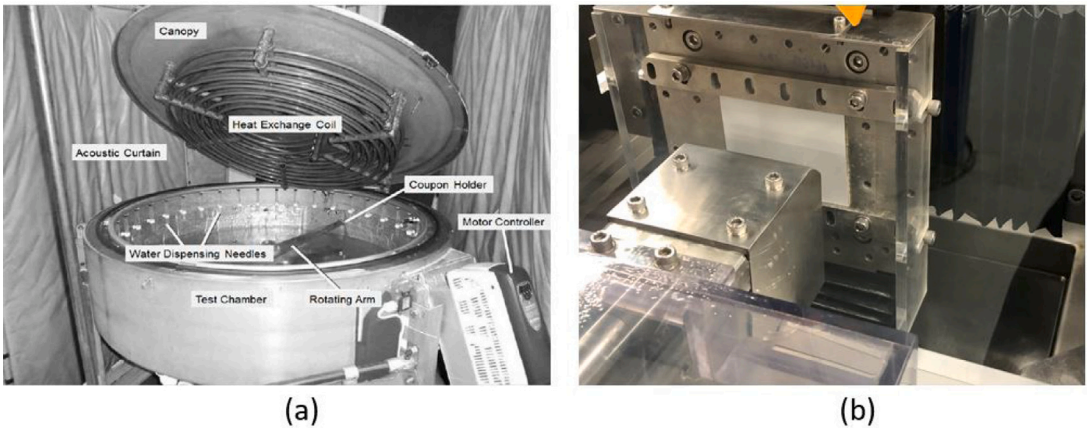

Fig. 2. (a) WARER (Whirling arm erosion tester) of the University of Limerick [23] (b) PJET (Pulsating Jet Erosion Tester) at Delft University of Technology.

patterns. However, the device maintains a fixed rain droplet diameter, rainfall speed, and continuous rainfall. In addition, the rotational speed of the arm can be adjusted as per the test requirements. The PJET, on the other hand, consists of a high-velocity water jet of which the diameter is defined through the nozzle diameter and the droplet length through a rotating disk with holes near the nozzle (a representative figure is shown later in Fig. 5(c)). This simulated droplet at high speed is targeted to the coated sample which is fixed in the tester. This test concept is similar to wind tunnel testing, where the sample is stationary and the air flow simulates the movement of the sample through the air. In the PJET, the droplet diameter, impact frequency, impact angle and impact velocity can be changed. Researchers suggest that the results from those two types of facilities cannot be directly correlated or compared [14], as the droplet impact mechanisms, the nature of the damaged area and the profile of the damage are very different for each test set-up [17,22].

One of the main challenges of using the PJET is the constant impact of waterjet segments on the sample, which occurs at a fixed frequency, velocity, and droplet size. It is important to note that this testing method may not accurately reflect the real-life rainfall conditions primarily for two reasons. (a) Firstly, in the test setup, the water jet is simulated continuously, whereas, in reality, there are always dry intervals between rain events. A dry interval refers to a period of no rainfall between two rain events. A representative example of this is shown in Fig. 3, where rainfall data at the Schiphol airport shows varying precipitation duration for 12 h of recorded data [24]. (b) Another reason that this testing method does not accurately reflect real-life rainfall conditions is that the impact frequency used in the test is generally kept high in the range of 30 to 40 Hz and is not in line with real rain intensities where impact frequency may range from 0.05 Hz to 5 Hz depending on the rainfall conditions [25]. An impact frequency is the duration between successive individual rain droplet impacts on a coated sample. Both these factors are critical when it comes to erosion testing of PU-based coatings that are visco-elastic in nature. For instance, the periods of dry intervals, in reality, may cause the visco-elastic material to recover part of its elastic response [26] and therefore withstand more impacts until failure compared to the scenario in the rain erosion tester (RET) where no dry intervals are simulated. In addition, different impact frequencies would present different relaxation times between droplet impacts, which may be crucial for visco-elastic materials. According to Engel et al. [26], if visco-elastic coatings have enough time for material recovery from one impact to the next one, the material would have time to dampen the impact energy as well as recover its impact absorbing capabilities before the next impact. However, if impact frequency is too high, recovery may not be possible, and strains may build up, leading to accelerated damage.

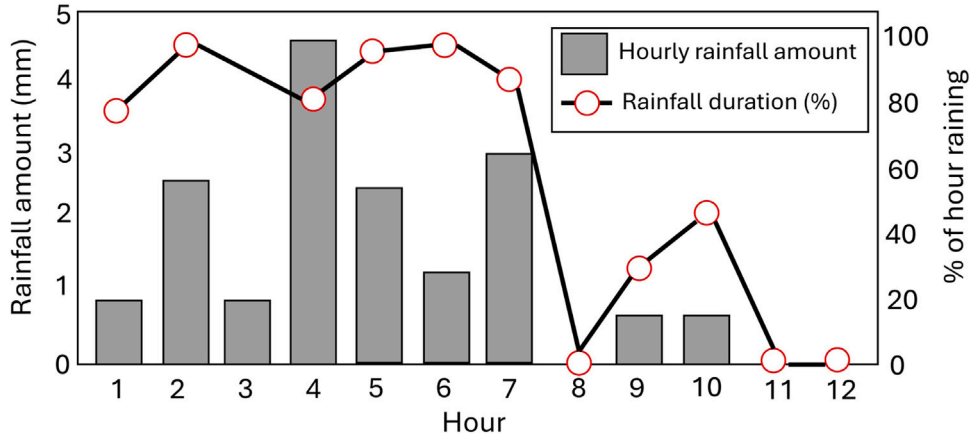

Fig. 3. Precipitation events during one day: KNMI: De Bilt, 22-05-2021.

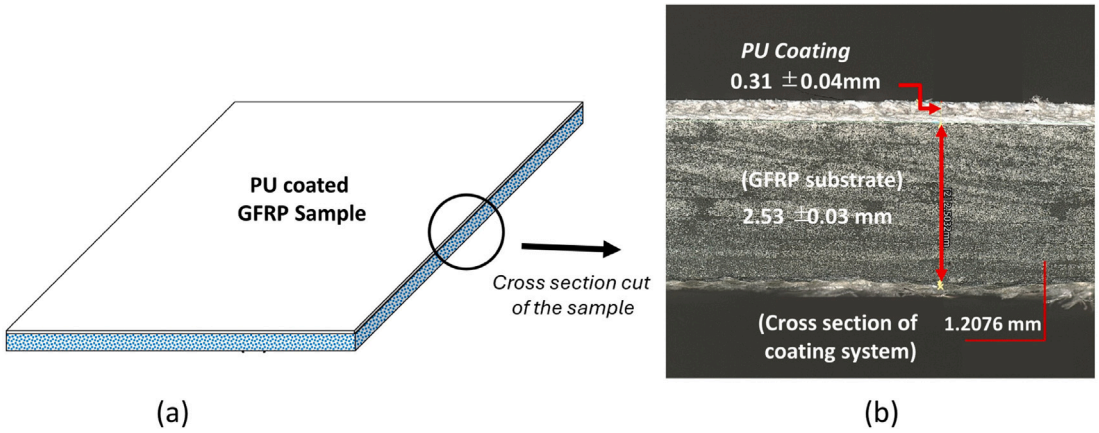

Fig. 4. Polyurethane (PU) coated glass fiber reinforced plastic (GFRP) sample: (a) global test sample (b) cross-section, including GFRP and PU thickness.

Currently, there are significant gaps in knowledge regarding how such uncertainty in the experimental modeling of erosion using PJET affects the results. The aim of this paper is, therefore, to investigate the effects of impact frequency and dry intervals on the incubation time of polyurethane-coated samples. An experimental study was conducted in a PJET where, firstly, the impact frequency and velocity were changed in the PJET facility to investigate the effect of impact frequency. Secondly, dry intervals were applied during the test procedure for a chosen frequency and velocity. The incubation time, which is the observation of the first visible damage, was measured in terms of the number of impacts until incubation (N) and the cumulative impact energy of the droplets until damage (J). Further, to analyze the test results, a new methodology is proposed for calculating the volume of water slug generated during the test and applied to PJET. After testing, the damaged features in the samples were studied via optical microscopy.

Novelty and structure of the paper

(a) The novelty of this research lies in its comprehensive approach to simulating and understanding rain erosion on polyurethane-coated samples, using two important parameters in PJET – impact frequencies and dry periods – which are overlooked in the design of experiments (DoE) using PJET. (b) We present an innovative theoretical model that accurately calculates the volume of water slugs at different impact velocities and frequencies. This model standardizes the erosive effects' comparison across a broad spectrum of testing conditions, a methodology introduced for the first time in this research. (c) The quantification of dry periods' effects on coating performance is articulated through three newly introduced PJET testing parameters: the duration of dry intervals, the rain exposure time preceding these intervals, and the number of dry intervals. This study is one of the first to quantify how these parameters affect the incubation period, thereby challenging the convention of continuous testing which may provide conservative, less realistic estimates. (d) The outcomes of this research provide a recalibrated approach to designing PJET testing campaigns, ensuring that test parameters better mimic the cyclic nature of real-world rainfall, thereby improving predictive models for material degradation. The structure of the paper is as follows: Section 2 describes the experiment. Section 3 describes the analysis procedure and parameters of interest. Section 4 presents the results and discussion. Finally, Section 5 concludes the paper.

2. Experiments

2.1. Sample preparation

Polyurethane (PU) coated samples were used in this study. The substrate consisted of Glass Fiber fiber-reinforced plastic (GFRP) manufactured by vacuum infusion (Fig. 4(a)). The GFRP plate was manufactured by Suzlon SE with a lay-up representing a realistic stacking sequence of the composite layers present at the leading edge of a wind turbine blade. The samples were then coated with a two-component PU coating (W4600) by 3M, as per the application guidelines, via cartridge and brush [27]. The glass transition temperature (T_g) of the coating is −5° [27]. The measured thickness (via cross-sectional microscopy) of the PU coating was 0.31 ± 0.04 mm in the tested samples, while the thickness of the substrate was 2.53 ± 0.03 mm (Fig. 4(b)). All samples

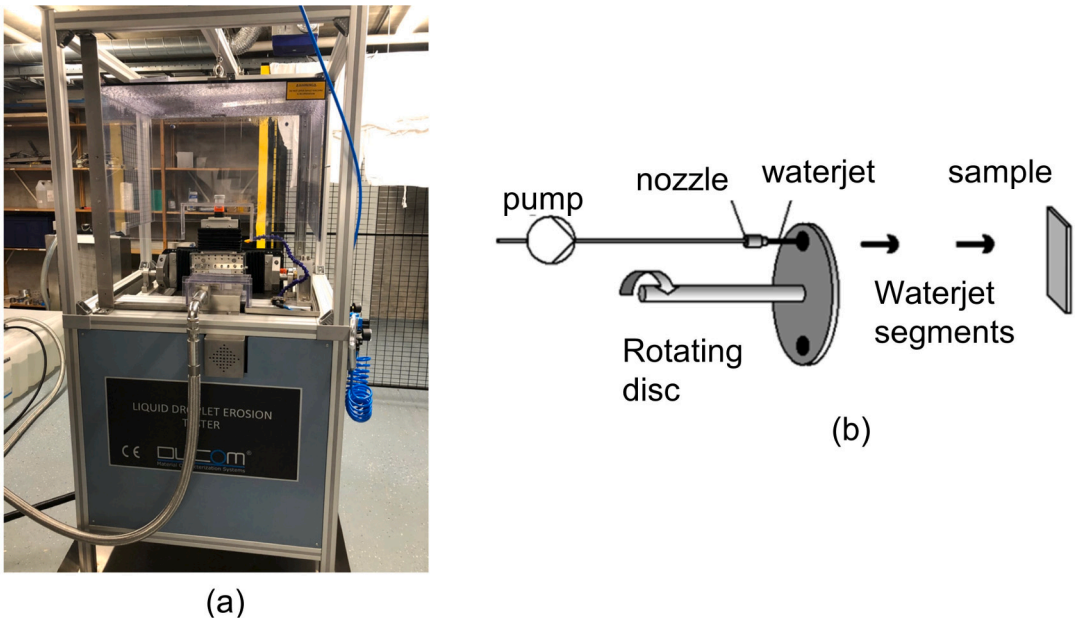

Fig. 5. (a) Pulsating Jet Erosion Tester (PJET) (b) PJET principle.

were subjected to a humidity treatment prior to testing in a climate chamber (CTS model LF7M04) at 38 °C and 95%RH for at least four days, to ensure that water uptake during testing did not influence the results and the samples were fully saturated.

2.2. Pulsating jet erosion tester

A PJET facility situated at the Delft University of Technology (TU Delft) (Fig. 5(a)) was used to simulate the repetitive water droplet impacts on coated samples. This facility accelerates rain erosion in coated samples and can be tested at different impact velocities and frequencies. It uses a high-pressure pump, which generates a continuous water jet through a nozzle at a certain velocity. The diameter of the droplets is determined by the chosen nozzle (1.5 mm diameter), which yielded a droplet diameter of 2 mm. This size was chosen as it is one of the most common droplet sizes used in research literature [28]. The water jet is then cut into water jet segments by a rotating disk with two holes at opposite sides of the disk, see Fig. 5(b). These water jet segments simulate the rain droplets. The frequency of water droplets is also set by the frequency of rotation of the rotating disk, therefore the change in the rotating disk frequency allows for the change in impact frequency. The distance from the nozzle to the sample was set to 50 mm. The impact angle was fixed at 90° to the sample, as research suggests that this is the most critical impact angle [29]. The structure where the sample is placed is covered by a transparent cabinet that allows the damage to be seen (see Fig. 5(a)). This cabinet remained closed while testing. In the test chamber, an air blower was also used to remove the water cushion film that may be present on the sample just after a droplet impact and may dampen the next droplet hit. The air supply pressure was set to 2 bar, which ensured the removal of the water cushion, which was validated through high-speed video footage. The water temperature in the PJET was stabilized through a cooler system. K-type thermocouples were placed on the sample in the test chamber and the water tank to measure the temperature during all tests. During the experiments, it was observed that the measured incubation times were longer at a lower temperature. Therefore, the measurements of incubation time were considered valid only when the water temperature was between 33–36 °C.

Table 1
Impact velocities and impact frequencies tested.

Impact velocity (m/s)	Impact frequency (Hz)
140	2.5, 27.7, 42.6
150	2.5, 27.7, 42.6
160	2.5, 27.7, 42.6
170	2.5, 27.7, 42.6
180	2.5, 27.7, 42.6

2.3. Description of parameters used in the rain erosion tests

Droplet impact frequency: Three different frequencies and five different impact velocities were chosen to test the effect of impact frequency on incubation; see Table 1. The velocities were selected to accelerate the testing but still represent the damage created by rain droplet impacts. The impact frequencies were chosen in the full range of the rotational frequencies of the rotating disk of the PJET, yielding impact frequencies of 2.5, 27.7, and 42.6 Hz. These would yield maximum relaxation times of 0.4, 0.036, and 0.023 s, respectively. All frequencies represent a heavy rainfall intensity [30,31], ranging from 24 to 31 l/h.

Dry periods: Instead of continuous rainfall, as typically used in PJET testing, the effect of dry periods and associated parameters on the incubation times were tested. Three rain characteristics were identified: dry period duration, time of rainfall before the dry period, and the number of dry periods, all potentially having an influence on incubation. Therefore, three test parameters were defined: (a) the number of dry intervals (n_{di}), (b) the duration of the dry interval (t_{dur}), (c) the rain exposure time before the start of the dry interval (t_{ret}). The last two parameters are defined with respect to the incubation time measured with continuous testing (no dry intervals) t_{incr} for ease of comparison. The case with continuous testing will be called the baseline case in the results. One or five dry intervals were chosen for the number of dry intervals (n_{di}). The dry interval duration t_{dur} was chosen to be either the incubation time or 5 times the reference incubation time, allowing for long term relaxation in the latter case. The rain exposure time before the start of the dry interval t_{ret} was chosen to be 0.2 or 0.5 times the reference incubation time, ensuring the incubation time was not reached before the dry interval. The impact frequency was set at 27.7 Hz and the impact velocity at 160 m/s for the dry interval testing. The levels chosen for the three parameters are shown in

Table 2
Parameters tested for dry intervals, with t_{incr} the reference incubation time with continuous testing (no dry intervals) in the PJET facility.

Duration of the dry interval t_{dur} [min]	Rain exposure time t_{rec} [min]	Number of dry intervals n_{di} [–]
$1 \times t_{incr} = 3.5$	$0.2 \times t_{incr} = 0.7$	1
$5 \times t_{incr} = 17.5$	$0.5 \times t_{incr} = 1.75$	5

Table 2, for which a full-factorial design of experiments was performed to investigate the influence of the three dry interval parameters on the incubation. A confidence interval of 95% was used for the analysis (α = 0.05). To assess the significance of the parameters, p-values were used. The p-values for each term were compared with the significance level α = 0.05. If the p-value for a term is lower than α (0.05), the association between this term and its response is statistically significant.

There are a few limitations of the study that need to be taken into account when extrapolating the results to real-life conditions: (1) The dry intervals in the PJET tester take place in a humid environment and therefore do not take into account the water absorption and adsorption that could take place in real-life conditions. Based on the DMA data, the E' and E" of the dry coating are higher than those of the wet coating and yield a smaller recovery time for the coating in case it is dry, thereby yielding longer incubation times. (2) On top of that, we tested the samples at only one rain intensity (frequency) and one droplet diameter, and the impact was generated on one spot of the sample. While this allows for accurate measurement of the effect of dry intervals, it is not representative of real-life conditions. For instance, higher impact frequencies would potentially lead to lower incubation times, as shown in the first part of the study. (3) The frequency considered in the relaxation times of the coating is related to the frequency of droplet impact, not the strain rates experienced by the coating materials and the different frequencies through coating thickness, which are much higher than the regime typically considered [32]. Although there are stress waves throughout the thickness of the coating, the main stress build-up is close to the surface and to the impact location [33]. The results from the study on dry intervals are therefore considered to be on the conservative side.

3. Analysis parameters and methods

3.1. Incubation time

The incubation time is defined as the moment when the first damage is visually observed in the sample [34]. The transparent cabinet of the PJET allows for observation of the samples while testing and spotting early features of damage. To measure the incubation time (rain erosion test time) [s], first, a chronometer is started once the set impact velocity is reached. When the first signs of damage appear, the chronometer is stopped. This is the end of the incubation period and is logged as the incubation time or testing time until damage [s]. The sample is then inspected for damage. If the damage observed is too large, then it is not considered in the data presented as it does not reflect the end of incubation accurately.

The incubation will be assessed in the results as the number of impacts until incubation (N) and the cumulative impact energy of the droplets until damage (J). The number of impacts until incubation (N) is calculated by multiplying the incubation time [s] by the impact frequency [Hz]. The incubation of the dry interval tests will be defined as the time when the sample was subjected to rain droplets only and thus does not include the dry periods. Therefore, we will represent the results as the number of impacts until incubation.

The kinetic energy of a droplet E_d [J] can be calculated based on the following formula:

$$E_d = \frac{1}{2} \cdot \rho \cdot V_{droplet} \cdot v_i^2 \tag{1}$$

where $V_{droplet}$ is the volume of the droplet, ρ is the density of the water (994.2 kg/m^3 on average at a water temperature of 33–36 °C), and v_i the impact velocity. The cumulative kinetic energy E_k is calculated by multiplying E_d with the number of impacts (N) defined above.

3.2. Calculation of volume of water slug

The volume of the water slug generated during the test ($V_{droplet}$) is dependent on the impact velocity and the impact frequency. Normally, for the calculation of the volume of the water slug, a cylindrical shape is assumed, having a cross-sectional area of $\frac{1}{4}\pi d^2$, with d the droplet diameter, and its length is calculated using the effective time when the water jet passes through the hole and forms the water slug [35]. However, this calculation overestimates the volume since the cross-sectional area of an actual water slug varies over time. Therefore, a more accurate methodology for calculating the water droplet volume is proposed and is based on the movement of the hole of the rotating disk in the PJET with respect to the water jet. In this context, this approach is referred to as the "theoretical volume". calculation for the volume of the water slug. Firstly, an expression for the overlap region (see Fig. 6), corresponding to the cross-sectional area over time (t), has be constructed. The overlap region can be categorized into two regions: complete overlap region ($A_{complete}$) and incomplete overlap region ($A_{incomplete}$), see Fig. 6(b). As the geometry to calculate the volume is symmetric, only half of the geometry will be used to set up the calculations.

The initial position is taken as the point where the center of the hole overlaps with the center of the water jet, which is referred to as $t = 0$. The complete overlap region starts from $t = 0$ and ends at $t = t_0$ when the cross-sectional area will start to decrease i.e. two circles are internally tangent. The interval from time t_0 to T is the incomplete overlap region where T denotes the time at which the two circles no longer overlap each other i.e. they are externally tangent, see Fig. 6(c). The cross-sectional area of the complete overlap region ($A_{complete}$) is determined by the circle with the smallest radius, i.e., the hole in the disk, being πr_{hole}^2. Fig. 6(c) and (d) show the cross-sectional area in the incomplete overlap region ($A_{incomplete}$). It is described by the sum of the area of the circular sector ABC and ADC subtracted by the area of the diamond-shaped $ABCD$ in the equation:

$$A_{incomplete} = \frac{2\alpha}{360°}\pi r_j^2 + \frac{2\beta}{360°}\pi r_h^2 - 2\sqrt{s(s-r_j)(s-r_h)(s-2Rsin\frac{\theta}{2})} \tag{2}$$

where $\overline{AB} = \overline{BC} = r_j$ and $\overline{AD} = \overline{CD} = r_h$ represent the radius of the jet and the radius of the hole respectively. The distance between the two centers $\overline{BD}$ is $2Rsin\frac{\theta}{2}$ where R is the distance from the center of rotation to the center of the jet and to the center of the hole and θ is the angle between the center of the jet and the center of the hole from the center of rotation. Using law of cosines and sines, angle α and β are derived as:

$$\alpha = cos^{-1}\left(\frac{r_j^2 + (2Rsin\frac{\theta}{2})^2 - r_h^2}{4r_j Rsin\frac{\theta}{2}}\right) \tag{3}$$

$$\beta = sin^{-1}\left(\frac{r_j sin\alpha}{r_h}\right) \tag{4}$$

The third term in Eq. (2) consists of two identical triangles ($\triangle ABD$ and $\triangle CBD$) that make up a diamond shape where s is defined in reference to Heron's formula.

$$s = \frac{r_j + r_h + 2Rsin\frac{\theta}{2}}{2} \tag{5}$$

The time dependency of θ can be written as:

$$\theta = \omega \cdot t = \frac{f}{2} \cdot t \tag{6}$$

where ω is the angular velocity of the rotating disk, which is the impact frequency (f) divided by two as there are two holes in the rotating disk.

The volume of the droplet ($V_{droplet}$) is now calculated by integrating the flow rate over time, as shown in Eq. (7) below. The flow rate is

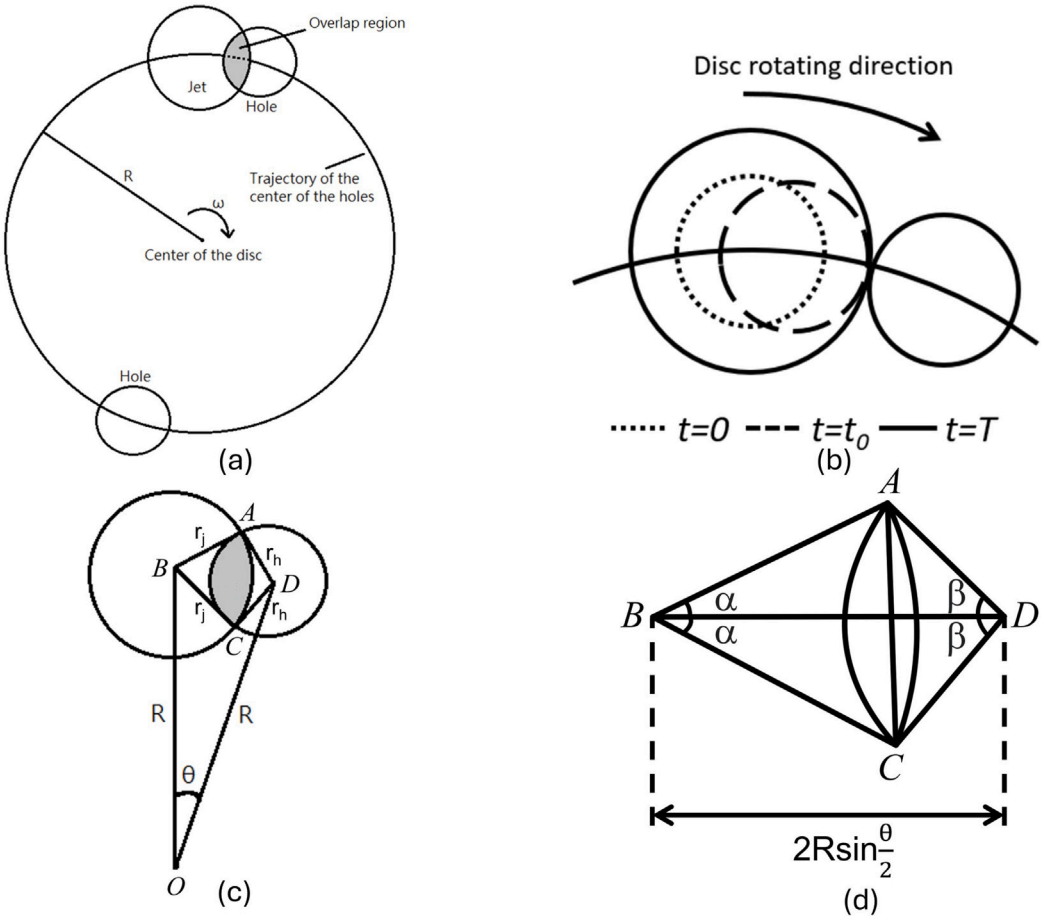

Fig. 6. (a) 2D geometry diagram of the disk, water jet and overlap region (b) rotation of the disk when the water jet overlaps the disk area: from t = 0 to t = T (c)(d) definition of the variables for calculations of overlap time and volume calculations.

the cross-sectional area (A) times the flow velocity (v_i). Lastly, the value should be doubled because only half of the traveling route was considered.

$$V_{droplet} = 2\int_0^T Avdt = 2v_i\left(\int_0^{t_0} A_{complete}dt + \int_{t_0}^T A_{incomplete}dt\right) \tag{7}$$

At $t = t_0$, $\overline{BD}$ is equivalent to the difference between the radii of the two circles, and at $t = T$, it is equivalent to the sum of the radii. Their expressions are shown below:

$$2Rsin\left(\frac{\omega t_0}{2}\right) = |r_j - r_h| \tag{8}$$

$$2Rsin\left(\frac{\omega T}{2}\right) = r_j + r_h \tag{9}$$

Further, t_0 and T can be derived as:

$$t_0 = \frac{2}{\omega}sin^{-1}\left(\frac{|r_j - r_h|}{2R}\right) \tag{10}$$

$$T = \frac{2}{\omega}sin^{-1}\left(\frac{r_j + r_h}{2R}\right) \tag{11}$$

3.3. Wö hler curves

To visualize the effect of frequency and velocity, Wöhler curves based on velocity (v_i) and number of impacts (N) have been constructed with a confidence interval of 95%. The $v_i - N$ curve can be represented assuming a power law:

$$N = k \cdot v_i^m \tag{12}$$

where k is a constant and m represents the slope of the Wöhler curve. The slope has been obtained using the least-squares method.

3.4. Analysis of damage features at incubation

A Keyence VR-5000 confocal microscope was used to evaluate the damage features and damaged area in tested samples (surface) and the thickness of the substrate and coating (cross-section). The microscope is capable of 3D imaging and measurement of the height map of the eroded area. For the initial assessment of the damages, a low magnification of 50x was used on a 15-inch monitor to obtain a wide field of view. However, for a more detailed evaluation of specific damage features, higher magnification and resolution settings of 80x on a 15-inch monitor were used. The height maps color palette was set at $[-0.015, 0.015]$ mm to allow for a general overview of the damage. Based on the height maps, a circular ring situated higher than the reference surface could be observed with an inner and outer radius. These radii were measured by fitting circles in the microscope's software, matching these two regions. The area of these circles is used to quantify the inner and outer damage area of the tested samples. The palette was changed to $[-0.004, 0.004]$ mm to observe more subtle changes in some damage features.

3.5. Analysis of visco-elastic behavior of bulk PU samples

Dynamic Mechanical Analysis (DMA) tests, using RSA-G2 Solids Analyzer, were performed to characterize the material and observe the visco-elastic behavior of bulk PU samples. Tensile clamp testing was considered the most suitable set-up due to the small thickness of

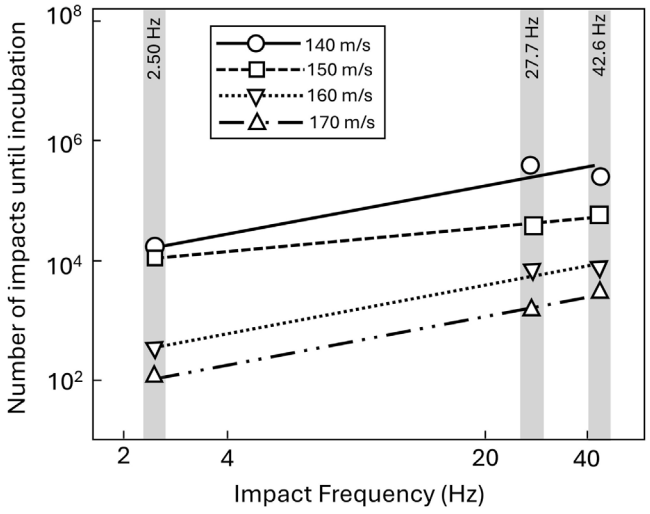

Fig. 7. Number of impacts until incubation – initial damage – as a function of impact frequency for different impact velocities — measurements and power law fitting.

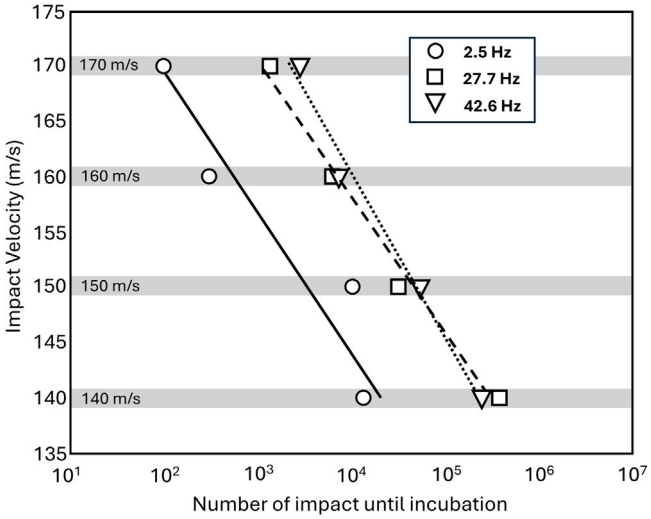

Fig. 8. v_i-N curves (impact velocity versus number of impacts until incubation) for different impact frequencies — measurements and power law fitting.

the bulk PU samples [36]. The dimensions of the sample were (63 ± 3) × (10±1) mm. The thickness of the tested samples was 0.60±0.05 mm. Tests were performed at 0.5 N static tensile axial load and with a dynamic load of 0.4 N. A frequency scan was carried out in the range from 1 to 20 Hz at a strain set at 0.1% and amplitude of 10 μm. The temperature was set at 45 °C, close to the actual temperature that the coating would undergo while testing. Although the frequencies used in this scan are much lower than the ones related to high-velocity impacts, low-frequency scans have been proven successful when assessing the change in properties of LEE PU coatings [37]. The changes in storage modulus (E') and loss modulus (E'') were measured. The DMA data showed relatively stable E′ and E″ values, slightly higher at higher frequencies as expected and gave at a frequency of 10 Hz of magnitude of the E′ and E″ of 36 MPa and 3.16 MPa respectively. The static properties of the coating are reported in [27].

4. Results and discussion

4.1. Droplet impact frequency

Fig. 7 shows the number of impacts until incubation that were obtained as a function of impact frequency and four impact velocities used in PJET. The results presented do not include the influence of the changes in mass of the droplet with different impact frequencies and velocities. It can be seen that increasing the impact frequency led to an increase in the number of impacts until incubation. This effect is observed for all impact velocities: for instance, the number of impacts until incubation for 42.6 Hz is 19 times larger than for 2.5 Hz for 140 m/s. Fig. 8 shows the Wöhler curves (velocity and number of impacts until incubation) for the different impact frequencies, showing a similar trend of increasing number of impacts for higher impact frequencies. This type of graph is typically used as a representation of the fatigue behavior of coated samples and is also used as input for the Springer's 1976 model [20,21,38–40]. The results did not yield significant differences in the slope of the v_i-N curves when changing the impact frequency. The typical dependency on impact velocity is seen with an increasing number of impacts until incubation for lower impact velocities.

The above results contradicted our initial hypothesis that a lower impact frequency would increase the number of impacts until incubation due to the visco-elastic behavior of the PU coating: the material would have larger short-time recovery between impacts, thereby decreasing strain build-up and delaying damage [25]. This is believed to be caused by the interdependence of the volume of the water slug from PJET that has significant dependence on the impact velocity and impact frequency, therefore disqualifying the typical representations of test results (of, for instance, v-n curves). Other analysis methods are proposed in this paper to observe the effect of impact frequency on the results based on cumulative kinetic energy and equivalent velocity. However, first, the interdependence of the impact velocity and frequency on the water slug volume is discussed below.

The interdependence of the impact velocity and frequency on the water slug volume is shown in Fig. 9(a)–(d), where theoretical calculation based on the volume calculations described in Section 3 is compared against the simplified cylindrical slug assumption. Fig. 9(a)–(c) compares the volumes of the water slug for different velocities and frequencies. It can be seen that making the assumption of a cylindrical slug overestimates the volume of water during each impact by slightly more than 2 times compared to theoretical estimates. In addition, it can also be seen that impact frequency has a larger effect than the impact velocity on the water volume within the test parameters used in the experimental campaign (Fig. 9(d)). It can also be observed that higher impact frequencies yield lower volumes compared to the lower impact frequencies, while a higher impact velocity yields higher impact volumes.

Next, we will consider the analysis of kinetic energy based on the theoretical volume of the water slug provided above. Based on the theoretical volumes, the kinetic energy of a droplet for each impact frequency and velocity can be calculated. Fig. 10 shows the theoretical energy of the droplet for the different impact velocities and frequencies used in the test campaign. It can be seen that high-impact frequencies yield low kinetic energy of the droplet, and high-impact velocities yield higher kinetic energy of the droplet. As with the volume of the slug, it can also be seen from the figure that the impact frequency also has the largest effect on the kinetic energy compared to impact velocity (within the range of the parameters used in the test campaign). Using the kinetic energy per impact shown above, the results for PJET can be shown in terms of cumulative kinetic energy E_k [J] (kinetic energy impacted upon the sample until incubation) versus impact velocity v_i for the different impact frequencies and is shown in Fig. 11. It can be seen that the results are close to each other for the different impact frequencies, with only a minor dependency shown for the results on impact frequency: for the same impact velocity, a lower impact frequency requires slightly more kinetic energy imparted on the sample to reach incubation. The dependency on velocity still as expected: lower

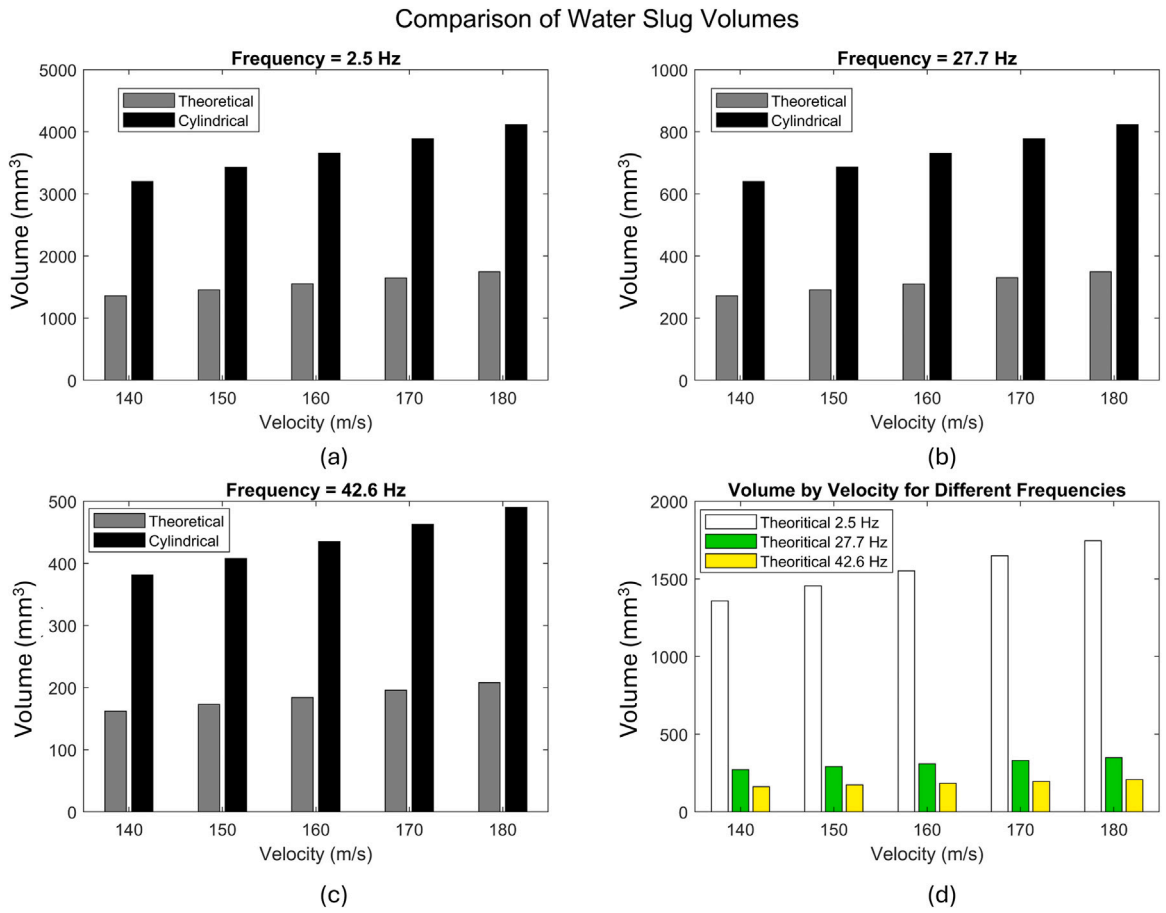

Fig. 9. Volume of water slug comparison between theoretical and cylindrical volume approximations.

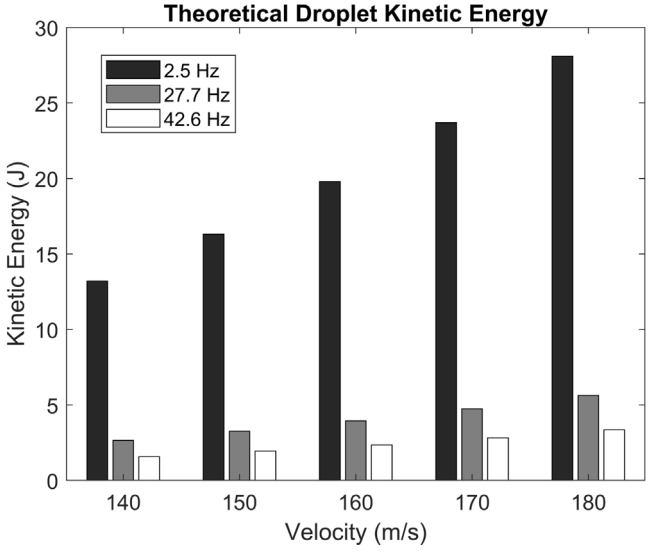

Fig. 10. Theoretical droplet kinetic energy for different velocities and frequencies.

cumulative kinetic energy needed at high impact velocities. As the impact velocity also influences the impact energy subjected to the samples, also this representation is not fully solving the interdependence of impact velocity and frequency and therefore does not allow for a proper comparison of the effect of the impact frequency only.

We, therefore, propose the concept of "equivalent velocity (v_{eq})" to compensate for the disregarded variation in volume (kinetic energy) in the current $v-n$ graph while maintaining a conventional representation of impact velocity with respect to a number of impacts until incubation. The equivalent velocity is based on using a consistent spherical reference droplet for the analysis. The droplet diameter (d) of this reference droplet is chosen to be 2 mm which is the diameter of the droplet used in the rain erosion tester. In general, the volume of a water slug produced by a high-speed water jet in the PJET is larger than that of a spherical water droplet with the same diameter. Consequently, the water slug also possesses greater kinetic energy than this spherical droplet at the same speed. The concept of "equivalent velocity" is to consider, with the reference droplet, how large the equivalent velocity should be to exert the same kinetic energy per impingement as the actual one in the experiment. Hence, the following equation can be written:

$$E_d = \frac{1}{2} m v^2 = \frac{1}{2} m_{ref} v_{eq}^2 \tag{13}$$

where m and v are the mass of the water slug and impact velocity in the PJET resp. and m_{ref} is the mass of the reference droplet, which can be expressed as:

$$m_{ref} = \frac{1}{6} \rho_L \pi d^3 \tag{14}$$

Therefore the equivalent velocity can be expressed as:

$$v_{eq} = \sqrt{\frac{m v^2}{m_{ref}}} \tag{15}$$

Overall, using the equivalent velocity to show the results, see Fig. 12, reduces the water slug volume interdependence with impact velocity and impact frequency. Two effects can be observed: a higher impact frequency yields lower amount of impacts until incubation, which also holds for a higher equivalent velocity. This implies that for the same

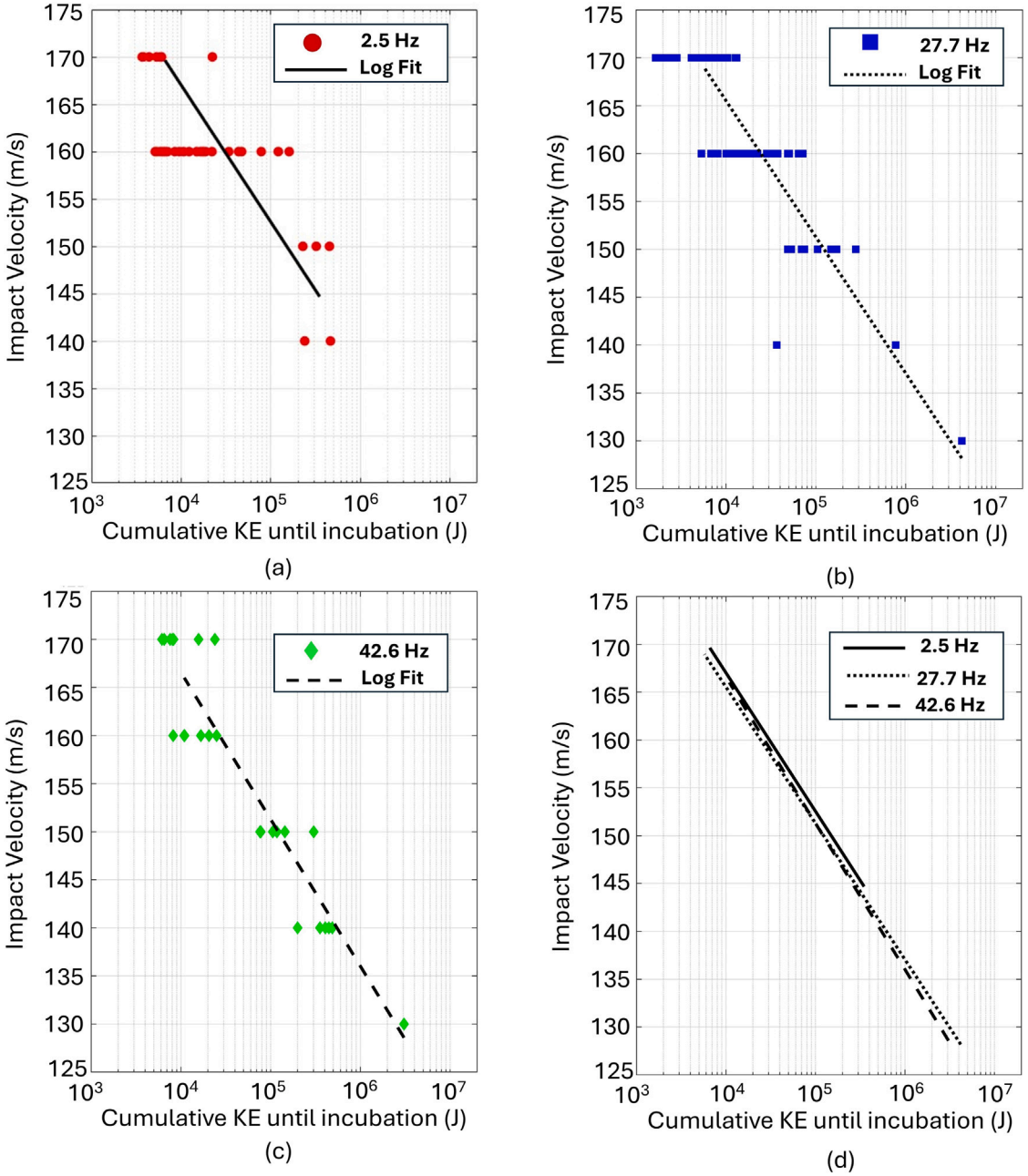

Fig. 11. Impact velocity versus cumulative kinetic energy v_i-E_k until incubation damage for different impact frequencies.

size of the droplet at the same equivalent velocity, the higher the impact frequency, the fewer the number of droplets are needed to cause damage. For instance, Fig. 13 shows a representative example where the incubation period for an equivalent impact velocity of 1000 m/s is compared for three impact frequencies. Here, the Wohler curves are extrapolated in both directions, and it can be clearly seen that the higher the impact frequency, the fewer the number of droplets are needed to cause damage. Also a lower Wöhler slope for the highest impact frequency can be seen, see Table 3. This observation aligns with the expectation of the recovery of deformation and visco-elastic behavior: as the impact frequency increases, the polyurethane coating has less time to recover from the strain, leading to faster erosion. Further, based on the DMA data, the relaxation time of the PU coating could be estimated (see Eqs. (16) and (17)), which has a frequency ω and temperature dependency. Using the storage modulus E' data from the frequency sweep at 45 °C and a simple Maxwell model, the relaxation time τ could be estimated using [41]:

$$E' = \frac{E\omega^2\tau^2}{1+\omega^2\tau^2} \tag{16}$$

With ω the angular frequency, τ the relaxation time of the polymer, E the Young's modulus. Further, using the loss modulus E'' data, the relaxation time could be estimated using:

$$E'' = \frac{E\omega\tau}{1+\omega^2\tau^2} \tag{17}$$

The calculated relaxation times were then extrapolated to the higher frequencies and listed in Table 4. The relaxation time of the polymer decreases with higher impact frequencies as the polymer behaves less viscous at these frequencies. The ratio between the maximum recovery time (the time between two impacts) given to the material and its relaxation time is also given in Table 4, where a higher number indicates more time for the polymer to recover and a number higher than 1

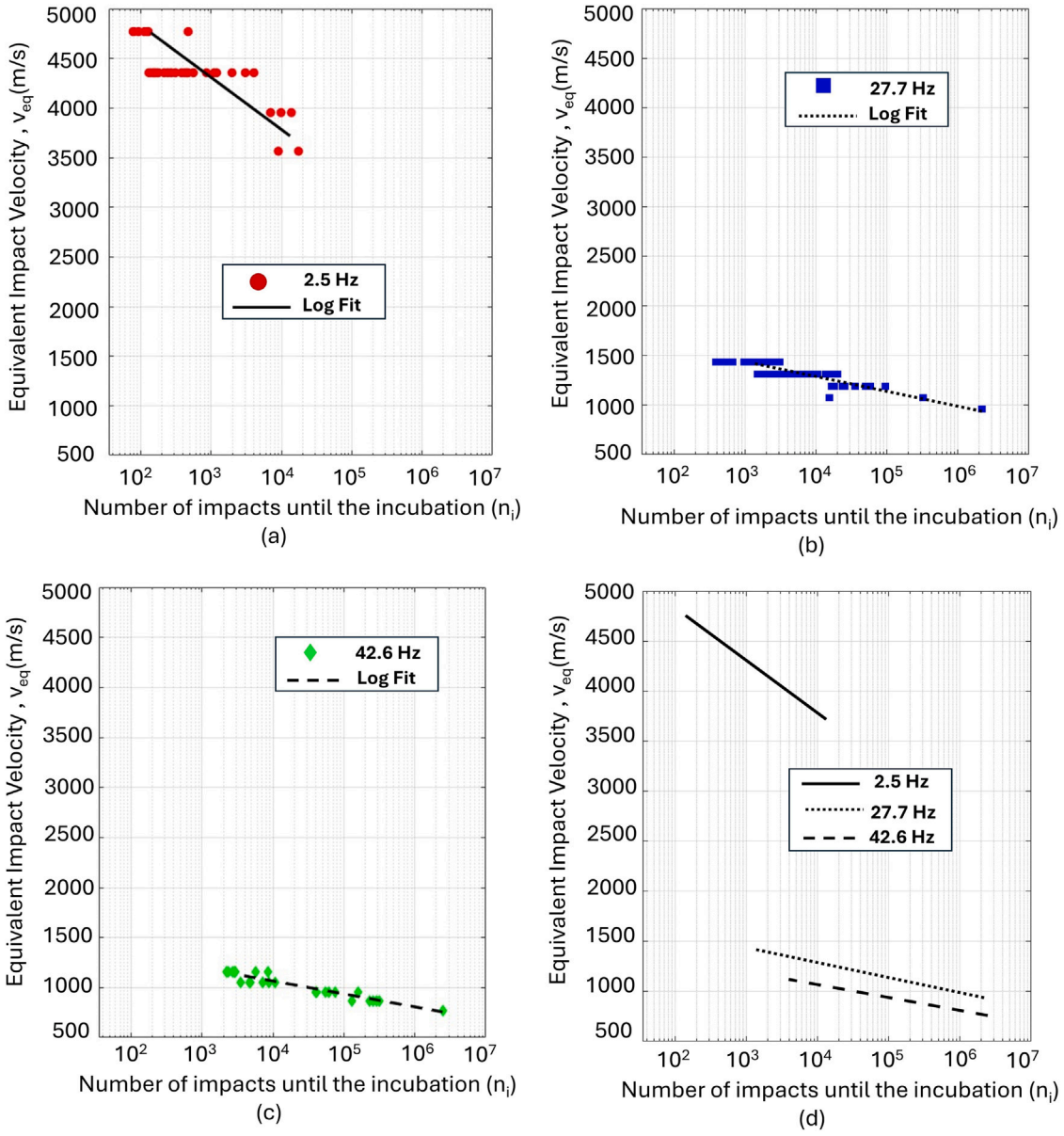

Fig. 12. Equivalent velocity with respect to the number of impacts until incubation for different impact frequencies.

Table 3
Slopes of the $v_{eq} - n_i$ curve corresponding to three impact frequencies.

f (Hz)	2.5	27.7	42.6
m (–, $v_{eq} - n_i$)	18.73	18.88	17.23

Table 4
Maximum recovery time during testing and relaxation times of material at different impact frequencies.

f (Hz)	2.5	27.7	42.6
Maximum recovery time during testing [sec]	0.4	0.036	0.023
Relaxation time PU based on E' [sec]	0.08	0.008	0.005
Relaxation time PU based on E'' [sec]	1.18	0.1	0.06
Ratio relaxation time (E') and recovery time [–]	5.1	4.4	4.3
Ratio recovery time and relaxation time (E'') [–]	0.34	0.36	0.36

indicating full recovery before the next impact. The time to recover for the elastic part of the polymer is larger for the lower frequencies of impact, while similar for all frequencies for the viscous part of the polymer.

4.2. Dry intervals

The effect of the dry intervals on the incubation periods and, more specifically, the duration of the dry interval, the rain exposure time before the start of the dry interval, and the number of dry intervals are shown in Fig. 14. Fig. 14(a) compares the incubation times for varying dry interval duration. For the longest dry interval of 17.5 min (five times the reference incubation time), we see an increase in incubation times up to five times compared to the baseline. However, even when the dry interval corresponds to a time corresponding to the reference incubation time, an increase of about 3.6 times was measured for the incubation time. This result is attributed to longer relaxation times for longer dry intervals for the PU coating, leading to better material recovery to its initial stress or strain state [42,43].

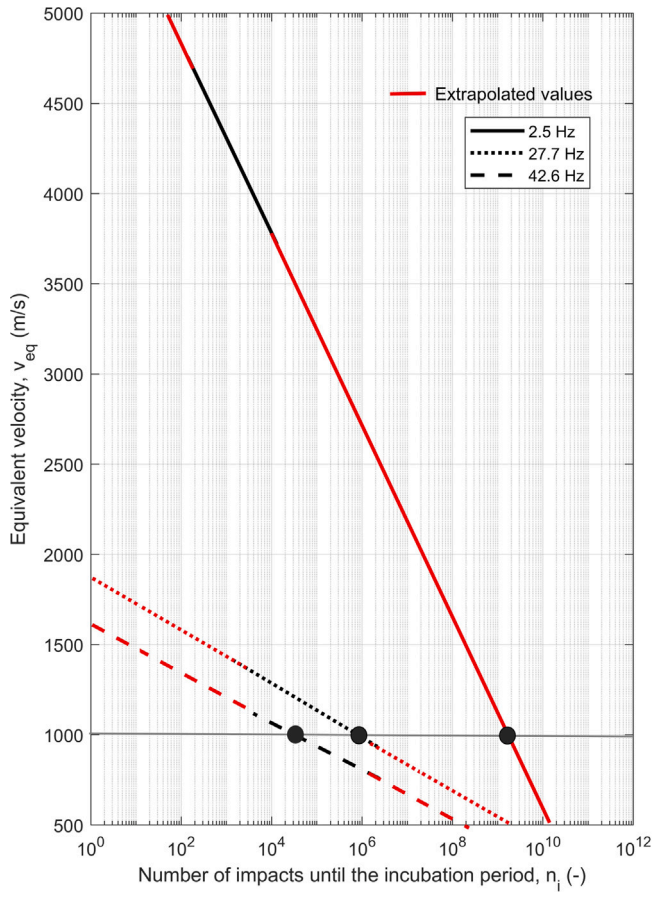

Fig. 13. Comparison of incubation period for the same equivalent impact velocity and different impact frequencies.

The rain exposure time before the start of the dry interval t_{ret} also has an influence, see Fig. 14(b). It was hypothesized that when the samples were subjected to rain for less time before the start of the dry interval, potentially less strain build-up and therefore less permanent deformation and more elastic recovery could be obtained. This would lead to an increase in incubation times. From the results, it can be observed that for the lowest value of t_{ret} about 4.8 times higher incubation times were obtained compared to the baseline. And even when the dry interval started after a higher rain exposure time, we still see an increase to about 3.8 times the incubation time. The number of dry intervals (n_{di}) also showed an increase of incubation times compared to the baseline (around 4.2–4.4 higher on average; see Fig. 14(c)). The number of dry intervals (1 or 5 dry intervals) did not show a significant difference in the results, as seen in Fig. 14(c). Also, the error bar in Figures 14(a)–(c) refers to the standard deviation of all the data points in the DoE. It can also be seen from the figures that standard deviations were higher when incubation times were higher. This can be attributed to the fact that local defects could lead to premature failures, which leads to higher standard deviations when the incubation times are higher.

These results are also confirmed by the results of the full-factorial analysis, summarized in Table 5. The p-values represent the significance of the low and high settings of each dry interval parameter. The p-values for the duration of the dry interval (t_{dur}) and rain exposure time before the start of the dry interval (t_{ret}), appear as significant, as they are smaller than the confidence interval (0.05). Therefore the dry interval parameters chosen are of importance to take into account when designing a proper test schedule in a PJET facility and when comparison studies are to be performed on different test rigs. From the analysis, it could also be concluded that the length of the dry interval had the largest influence on the increase in incubation time when dry intervals were introduced. All results of the dry interval parameters with respect to the continuous testing are statistically significant. Our results are in line with a study performed by Zhang et al. [17], where the incubation times of discrete straight jet (introducing dry intervals during testing) were significantly higher compared to a continuous flat fan jet. Our results could also partially explain why the PU coatings have a longer incubation time in whirling arm jet facilities (a dry period per rotation) compared to PJET testing [44,45].

Table 5
Statistical significance of the results with respect to time to incubation: p-values (based on significance level of 0.05).

Parameter	P-Values
t_{dur}	0.008
t_{ret}	0.027
n_{di}	0.578

The effect of the dry intervals was also measured in the surface damage and, more specifically, the size of the plastic ring observed after erosion testing, see Fig. 15. A representative Figure for the plastic ring size is given in Fig. 16. It can be seen that for a long dry interval (Fig. 15(a)), the damage is smaller than for the baseline, which corresponds to no dry intervals. No significant differences in plastic ring size are observed for the other parameters. Also, no differences in the damage features, such as pitting, cracks, and debonding, were observed for the different parameters. The diameter at which plastic deformation is observed seems to confirm that a longer time for recovery would lead to less or a smaller plastic damage area and lead to the highest incubation times. As the results of the other parameters do not show significant differences in damage (size), the results cannot be fully explained by the size of the plastic zone.

The results in fatigue improvement obtained when including dry intervals in this study seem similar to the results obtained for fatigue improvement obtained for work-hardened metals, where also a four times longer fatigue life was observed compared to the non-work-hardened metals [46]. Due to a local high stress in work-hardening, a plastic deformation at the start of the fatigue life was obtained. This led to stress reductions in the plasticized zone and the crack propagation could be delayed when the metal softens under the cyclic strain. Also the residual stresses imposed due to the plastic deformation could play a role in the resulting fatigue life. Kepert and Payne [47] showed that high static pre-loading to about 80%–90% of the ultimate strength of the material would result in 4 times longer fatigue life. Schijve et al. [48] found that when periodically overloading an aluminum riveted assembly in tension, beneficial compressive residual stresses are generated in the material, leading to an increased fatigue lifetime. Gafhoori et al. [49] showed that for notched steel bars reinforced with bonded carbon fiber reinforced plastic plates (CFRP), 20% of pre-stressing the CFRP material could even lead to a crack arrest in the notched samples [49].

An analogy can be made to erosion testing, where a plastic ring-like feature appears due to the first impacts of rain droplets on the coating. This results in a stretched surface and compressive stress in the coating, which in turn delays crack initiation. This is especially noticeable during dry interval testing, where the initial stress causing plastic deformation is temporarily removed, allowing the initial strain build-up to be released in the visco-elastic material. By increasing the recovery time (longer dry interval duration) and reducing the strain build-up time (shorter rain exposure time before the dry interval), a longer incubation time is achieved.

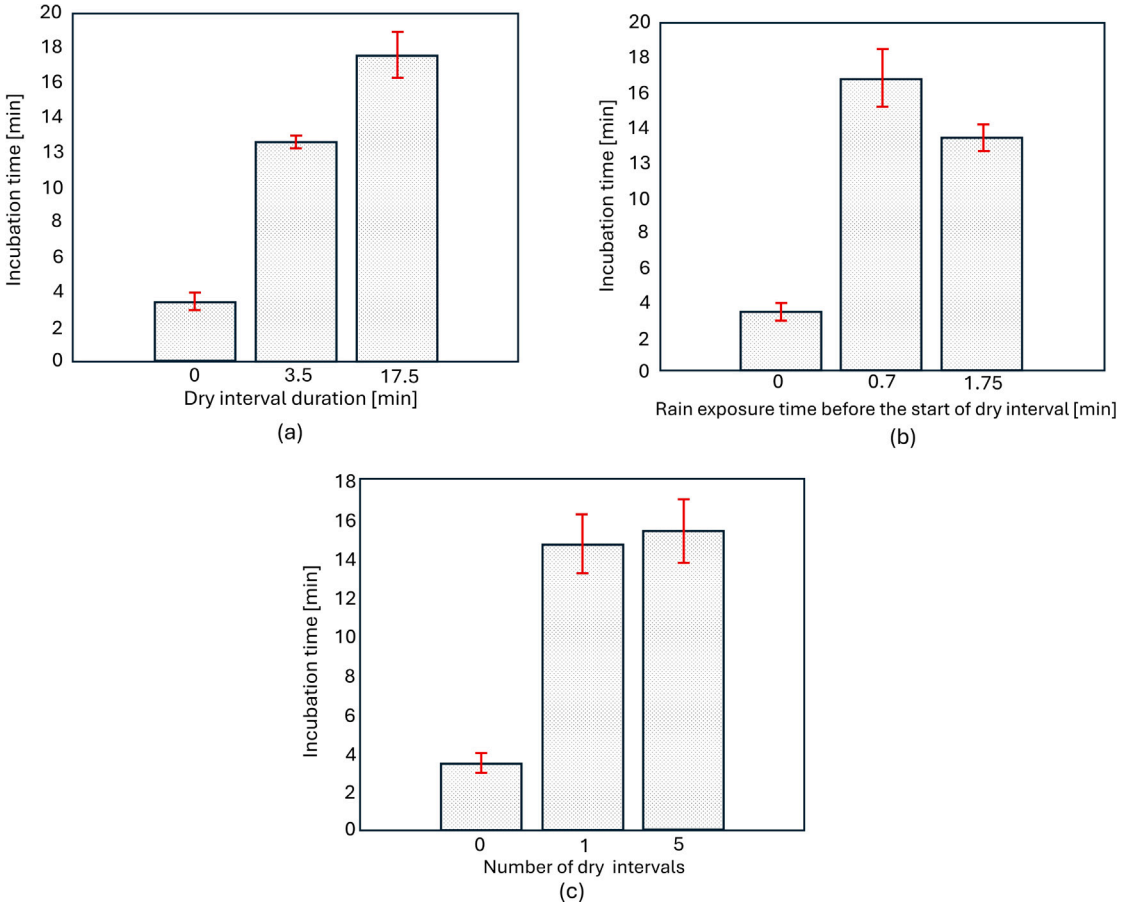

Fig. 14. Dry interval parameters with respect to incubation time (The error bar in these figures refers to the standard deviation of all the data points in the DoE.).

5. Conclusions & recommendations

This study investigates the impact of droplet impact frequencies and dry intervals on the incubation time for damage on polyurethane-coated samples using a Pulsating Jet Erosion Tester (PJET). The following are the main conclusions of the study:

Effect of droplet impact frequency on incubation periods of PU coating: A novel theoretical model accurately calculating the volume of water slugs at different impact velocities and frequencies, as well as the concept of equivalent velocity were introduced in this work to calculate and present the results of PJET. This allowed for compensating for the variation in rain droplet volume and hence its kinetic energy that was disregarded in the conventional representation of v-n graphs. Using this approach, it was possible to observe that the higher the impact frequency, the fewer droplets needed to cause damage in the coated samples. This observation was aligned with the expectation of the recovery of deformation and the physical visco-elastic behavior of the coating. Overall, as the impact frequency increases, the polyurethane coating has less time to recover from the strain, leading to faster erosion.

Effect of dry intervals on incubation periods of PU coating: Three parameters were tested: the duration of dry intervals, the rain exposure time preceding these intervals, and the number of dry intervals. The first two have an effect on the incubation time: a long dry interval duration and short rain exposure time before the dry interval have been found to have a positive effect. The effect of the dry intervals was also measured in terms of surface damage of the coating. Only the damage for a long dry interval was found smaller than for the baseline. Also, no differences in other damage features such as pitting, cracks, and debonding were observed for the different parameters. It was found that initial plastic deformation initiated upon droplet impact, when given time to relax, can improve the surface fatigue life significantly during PJET testing. This requires attention when comparing test results from different PJET testing and designing PJET test campaigns. It was also found that incubation times reported for continuous testing (i.e., without any dry intervals) are considered conservative when compared to real-life performance.

Recommendations for future studies:

- When investigating the effect of impact frequency, it is recommended to do a proper design of the test set-up and more specifically of the rotating disk through changing the amount of holes in the disk, to change the impact frequency, and changing the length and/or shapes of the holes to compensate for the droplet length change at different impact velocities.
- For comparison tests between different facilities, it is important to check the test parameters and ensure the PJET facility imparts a similar kinetic energy per droplet for each test velocity, compared to the other facility such as a whirling arm facility.
- Investigating the impact behavior of different impact spots next to each other, on how the plastic deformation of one spot influences the other spot and the effect of the incubation behavior of the different spots, for instance in a PJET with moving substrate or whirling arm set-up
- Investigating with a single droplet impact the effect of impact velocity and rain droplet diameter on the viscoelastic behavior and wave propagation in the coating

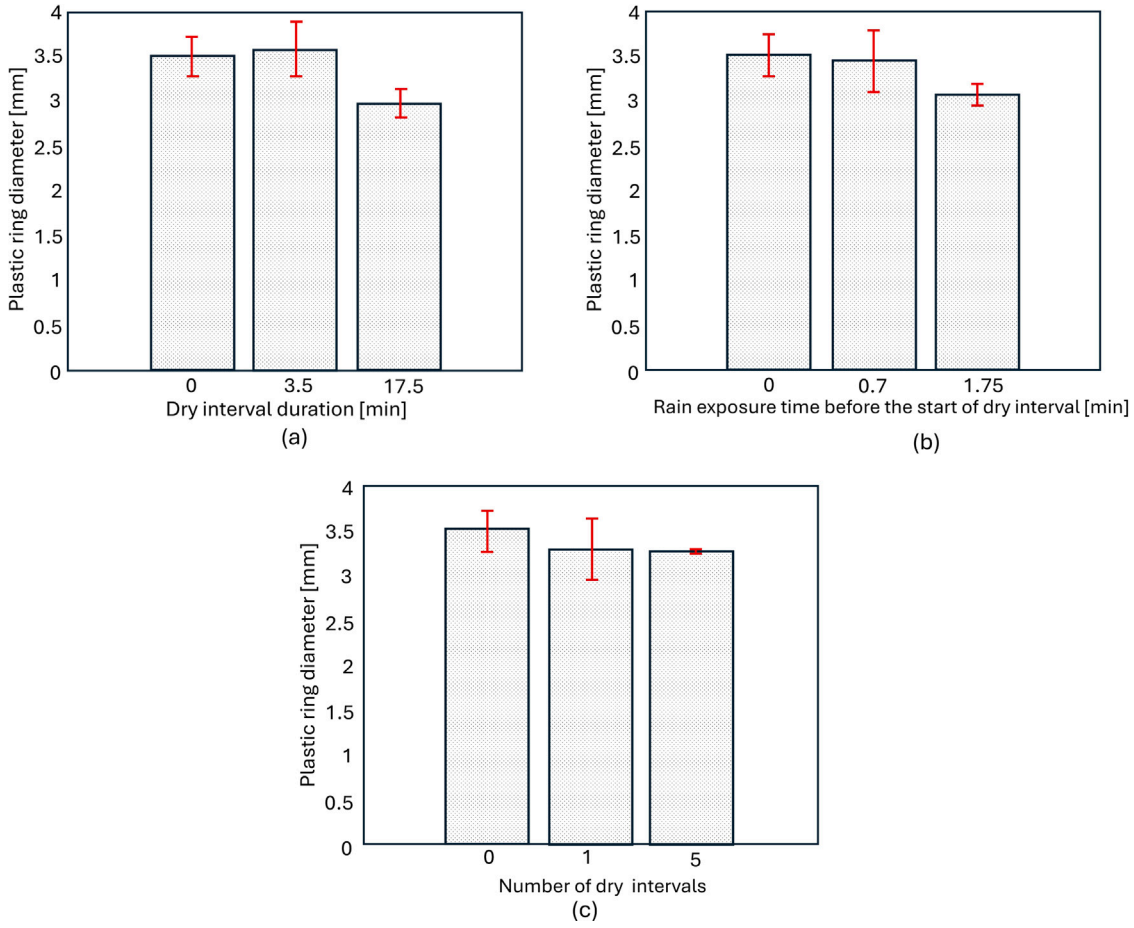

Fig. 15. Dry interval parameters with respect to inner diameter of plastic ring formation after incubation (The error bar in these figures refers to the standard deviation of all the data points in the DoE.).

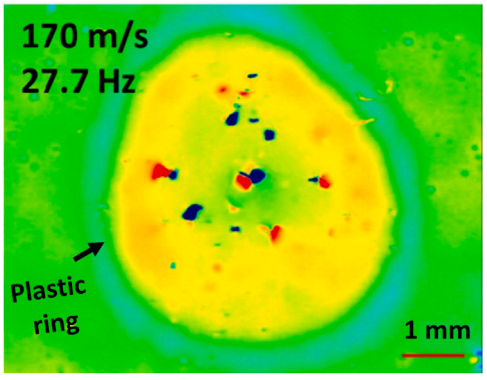

Fig. 16. Formation of a plastic ring on the coated sample during PJET testing.

- The effect of the coating drying during dry intervals and its effect on incubation could be further investigated.
- It is also recommended to investigate the effect of the parameters considered in this study on the damage progression post-incubation for PJET testing.

CRediT authorship contribution statement

Amrit Shankar Verma: Writing – review & editing, Writing – original draft, Supervision, Project administration, Methodology, Investigation, Funding acquisition, Formal analysis, Data curation, Conceptualization. **Chun-Yen Wu:** Writing – review & editing, Methodology, Investigation, Formal analysis, Data curation, Conceptualization. **Miguel Alonso Díaz:** Writing – original draft, Software, Methodology, Investigation, Formal analysis, Data curation, Conceptualization. **Julie J.E. Teuwen:** Writing – review & editing, Writing – original draft, Supervision, Project administration, Methodology, Investigation, Formal analysis, Data curation, Conceptualization.

Declaration of competing interest

The authors declare that they have no known competing financial interests or personal relationships that could have appeared to influence the work reported in this paper.

Acknowledgment

The first author of the paper acknowledges the startup funds provided by the Office of Vice President and Research (OVPR), University of Maine, USA.

Data availability

Data will be made available on request.

References

[1] Wind energy in Europe-2020 statistics and the outlook for 2021–2025, 2021, https://s1.eestatic.com/2021/02/24/actualidad/210224_windeurope_combined_2020_stats.pdf. (Accessed 24 November 2021).

[2] How much wind was in Europe's electricity yesterday?, 2023, https://windeurope.org/about-wind/daily-wind/. (Accessed 02 October 2023).

[3] Offshore wind market report: 2023 edition, figure 35, p.75, 2023, https://www.energy.gov/sites/default/files/2023-09/doe-offshore-wind-market-report-2023-edition.pdf. (Accessed 02 October 2023).

[4] Animation: Visualizing the world's biggest wind turbines, 2022, https://elements.visualcapitalist.com/animation-visualizing-the-worlds-biggest-wind-turbines/. (Accessed 02 October 2023).

[5] H. Macdonald, D. Infield, D.H. Nash, M.M. Stack, Mapping hail meteorological observations for prediction of erosion in wind turbines, Wind Energy 19 (4) (2016) 777–784.

[6] M.S. Campobasso, A. Castorrini, L. Cappugi, A. Bonfiglioli, Experimentally validated three-dimensional computational aerodynamics of wind turbine blade sections featuring leading edge erosion cavities, Wind Energy 25 (1) (2022) 168–189, http://dx.doi.org/10.1002/we.2666.

[7] L. Mishnaevsky Jr., Toolbox for optimizing anti-erosion protective coatings of wind turbine blades: Overview of mechanisms and technical solutions, Wind Energy 22 (11) (2019) 1636–1653.

[8] Z. Ren, A.S. Verma, Y. Li, J.J. Teuwen, Z. Jiang, Offshore wind turbine operations and maintenance: A state-of-the-art review, Renew. Sustain. Energy Rev. 144 (2021) 110886, http://dx.doi.org/10.1016/j.rser.2021.110886, URL https://www.sciencedirect.com/science/article/pii/S1364032121001805.

[9] A.S. Verma, S.D. Noi, Z. Ren, Z. Jiang, J.J. Teuwen, Minimum leading edge protection application length to combat rain-induced erosion of wind turbine blades, Energies 14 (6) (2021) 1629.

[10] M.H. Keegan, D. Nash, M. Stack, Wind Turbine Blade Leading Edge Erosion: An Investigation of Rain Droplet and Hailstone Impact Induced Damage Mechanisms (Ph.D. thesis), University of Strathclyde, 2014.

[11] http://www.duraledge.dk. Picture taken under permission from duraledge project.

[12] https://www.tno.nl, Picture taken under permission from tno.

[13] T. Yamagata, M. Hasegawa, N. Fujisawa, Erosion behavior of pulsed-jet test facility for wind turbine blade, Wear 514–515 (2023) 204565, http://dx.doi.org/10.1016/j.wear.2022.204565.

[14] E. Tobin, T. Young, D. Raps, O. Rohr, Comparison of liquid impingement results from whirling arm and water-jet rain erosion test facilities, Wear 271 (9–10) (2011) 2625–2631.

[15] E. Tobin, O. Rohr, D. Raps, W. Willemse, P. Norman, T. Young, Surface topography parameters as a correlation factor for liquid droplet erosion test facilities, Wear 328–329 (2015) 318–328, http://dx.doi.org/10.1016/j.wear.2015.02.054.

[16] S. Zhang, K. Dam-Johansen, P.L. Bernad, S. Kiil, Rain erosion of wind turbine blade coatings using discrete water jets: Effects of water cushioning, substrate geometry, impact distance, and coating properties, Wear 328–329 (2015) 140–148, http://dx.doi.org/10.1016/j.wear.2015.01.079.

[17] S. Zhang, K. Dam-Johansen, S. Nørkjær, P.L. Bernad Jr., S. Kiil, Erosion of wind turbine blade coatings–design and analysis of jet-based laboratory equipment for performance evaluation, Prog. Org. Coat. 78 (2015) 103–115.

[18] A. Shankar Verma, Z. Jiang, Z. Ren, M. Caboni, H. Verhoef, H. van der Mijle-Meijer, S.G. Castro, J.J. Teuwen, A probabilistic long-term framework for site-specific erosion analysis of wind turbine blades: A case study of 31 Dutch sites, Wind Energy (2021).

[19] A. O'Carroll, Correlation of mechanical properties to rain erosion resistance of polymeric materials, 2018.

[20] R. Herring, L. Domenech, J. Renau, A. Šakalytė, C. Ward, K. Dyer, F. Sánchez, Assessment of a wind turbine blade erosion lifetime prediction model with industrial protection materials and testing methods, Coatings 11 (7) (2021).

[21] J.I. Bech, N.F.-J. Johansen, M.B. Madsen, Á. Hannesdóttir, C.B. Hasager, Experimental study on the effect of drop size in rain erosion test and on lifetime prediction of wind turbine blades, Renew. Energy 197 (2022) 776–789.

[22] B. Luiset, F. Sanchette, A. Billard, D. Schuster, Mechanisms of stainless steels erosion by water droplets, Wear 303 (1–2) (2013) 459–464.

[23] I. Katsivalis, A. Chanteli, W. Finnegan, T.M. Young, Mechanical and interfacial characterisation of leading-edge protection materials for wind turbine blade applications, Wind Energy 25 (10) (2022) 1758–1774, http://dx.doi.org/10.1002/we.2767, arXiv:https://onlinelibrary.wiley.com/doi/pdf/10.1002/we.2767, URL https://onlinelibrary.wiley.com/doi/abs/10.1002/we.2767.

[24] Uurgegevens van het weer in Nederland KNMI, https://www.knmi.nl/nederland-nu/klimatologie/uurgegevens. (Accessed 2 August 2021).

[25] A. Conn, S. Rudy, Effects of fatigue and dynamic recovery on rain erosion, in: Erosion, Wear, and Interfaces with Corrosion, ASTM International, 1974.

[26] O.G. Engel, Waterdrop collisions with solid surfaces, J. Res. Natl. Bur. Stand. 54 (5) (1955) 281–298.

[27] Blade protection coating W4600 - Technical data sheet and application guide, 2014, https://multimedia.3~m.com/mws/media/978868O/3m-wind-blade-coating-w4600-app-guide-and-technical. (Accessed 17 April 2021).

[28] M. Elhadi Ibrahim, M. Medraj, Water droplet erosion of wind turbine blades: Mechanics, testing, modeling and future perspectives, Materials 13 (1) (2020) 157.

[29] A.S. Verma, S.G. Castro, Z. Jiang, J.J. Teuwen, Numerical investigation of rain droplet impact on offshore wind turbine blades under different rainfall conditions: A parametric study, Compos. Struct. 241 (2020) 112096.

[30] Water - National meteorological library and archive fact sheet 3 - Water in the atmosphere, 2012, p. 17, https://www.metoffice.gov.uk/binaries/content/assets/metofficegovuk/pdf/research/library-and-archive/library/publications/factsheets/factsheet_3-water-in-the-atmosphere-v02.pdf. (Accessed 05 October 2023).

[31] R. Herring, K. Dyer, P. Howkins, C. Ward, Characterisation of the offshore precipitation environment to help combat leading edge erosion of wind turbine blades, Wind Energy Sci. 5 (4) (2020) 1399–1409.

[32] S. Doagou-Rad, L. Mishnaevsky, Rain erosion of wind turbine blades: computational analysis of parameters controlling the surface degradation, Meccanica 55 (2020) 725–743.

[33] C.B. Burson-Thomas, T.J. Harvey, L. Fletcher, R. Wellman, F. Pierron, R.J.K. Wood, Investigating high-speed liquid impingement with full-field measurements, Proc. R. Soc. Lond. Ser. A Math. Phys. Eng. Sci. 47920230023 (2023).

[34] H. Slot, E. Gelinck, C. Rentrop, E. Van Der Heide, Leading edge erosion of coated wind turbine blades: Review of coating life models, Renew. Energy 80 (2015) 837–848.

[35] T.H. Hoksbergen, Predicting Rain Erosion Damage in Wind Turbine Blade Coating Materials (Ph.D. thesis), University of Twente, 2023.

[36] D. Dunson, Characterization of polymers using dynamic mechanical analysis (DMA), EAG Appl. Note (2017).

[37] I. Ouachan, M. Kuball, D. Liu, K. Dyer, C. Ward, I. Hamerton, Understanding of leading-edge protection performance using nano-silicates for modification, in: Journal of Physics: Conference Series, Vol. 1222, IOP Publishing, 2019, 012016.

[38] M.E. Ibrahim, M. Medraj, Prediction and experimental evaluation of the threshold velocity in water droplet erosion, Mater. Des. 213 (2022) 110312.

[39] S. Fæster, N.F.-J. Johansen, L. Mishnaevsky Jr., Y. Kusano, J.I. Bech, M.B. Madsen, Rain erosion of wind turbine blades and the effect of air bubbles in the coatings, Wind Energy 24 (10) (2021) 1071–1082.

[40] G.S. Springer, Erosion by liquid impact, 1976.

[41] D.I. Bower, An introduction to Polymer Physics, Cambridge University Press, 2002.

[42] L.P. Young R.J., Introduction to Polymers, second ed., CRC Press, 1991, p. 329.

[43] A.V. Cowie J.M.G., Polymers: Chemistry and Physics of Modern Materials, third ed., CRC Press, 2008, p. 365.

[44] E.F. Tobin, T.M. Young, D. Raps, Evaluation and correlation of inter-laboratory results from a rain erosion test campaign, in: Proceedings of 28th International Congress of the Aeronautical Sciences, 2012.

[45] E.F. Tobin, O. Rohr, D. Raps, W. Willemse, P. Norman, T.M. Young, Surface topography parameters as a correlation factor for liquid droplet erosion test facilities, Wear 328 (2015) 318–328.

[46] W. Barrois, Repeated plastic deformation as a cause of mechanical surface damage in fatigue, wear, fretting-fatigue, and rolling fatigue - A review, Int. J. Fatigue 1 (1979) 167–189.

[47] J.L. Kepert, P.A. O., Interim Report on Fatigue Characteristics of a Typical Metal Wing (NACA-TM-1397), Tech. Rep., NTRS - NASA Technical Reports Server, 1956.

[48] J. Schijve, Fatigue of Structures and Materials, second ed., Springer, 2009, pp. 295—-328.

[49] E. Ghafoori, A. Schumacher, M. Motavalli, Fatigue behavior of notched steel beams reinforced with bonded CFRP plates: Determination of prestressing level for crack arrest, Eng. Struct. 45 (2012) 270–283.